Supporting Information:

Boosting Oxygen Evolution Activity of NiFe-LDH Enabled by Oxygen Vacancy and Morphological Engineering

Shuxuan Liu[#a], Huiwen Zhang[#a], Enlai Hu[#a], Tuyuan Zhu[a], Chunyan Zhou[a], Yingchong Huang[a], Min Ling[b], Xuehui Gao[a]* and Zhan Lin[c]

[a] Department of Chemistry, Key Laboratory of the Ministry of Education for Advanced Catalysis Materials, Zhejiang Normal University, Jinhua 321004, China.

[b] College of Chemical and Biological Engineering, Zhejiang University, Hangzhou 310027, China.

[c] Guangzhou Key Laboratory of Clean Transportation Energy Chemistry, School of Chemical Engineering and Light Industry, Guangdong University of Technology, Guangzhou Higher Education Mega Center, Guangzhou 510006, Guangdong, China.

Materials characterization

Field emission scanning electron microscopy (FESEM) images of the synthesized materials were collected on the Hitachi S-4800. The microstructure of the electrocatalysts was elucidated using the transmission electron microscopy (TEM) on JEM-2100F. The crystal structures of the electrocatalysts were identified by using X-ray powder diffraction (XRD) measurement with a D8 Advance X-ray diffractometer (Bruker AXS). X-ray photoelectron spectroscopy (XPS) of the materials was analyzed by using the ESCALAB-250Xi. The Quantachrome gas adsorption analyzer (USA) determined the specific surface area and pore size distribution of the samples, and data analysis was performed by using the corresponding Brunauer-Emmett-Teller (BET) method and N_2 adsorption/desorption measurement with Quantachrome software. Electron Paramagnetic Resonance (EPR) measurement was obtained on the Bruker EPR EMXplus-9.5/12 at room temperature. Raman curves were collected on Renishaw RM100003040405 Raman spectrometer (Hong Kong) using the 532 nm laser line, and the exposure time and the power are 10 s and 0.5%, respectively.

Electrochemical measurement

Fabrication of working electrodes.

First, nickel foam (NF, 1.0 ~ 1.5 cm^2) was pretreated to remove the oxide layer and impurities on the surface. NF was washed in 3 M HCl, DI and ethanol by continuous ultrasonic, and then naturally dried in the air. The electrocatalyst, carbon black (Super P) and polyvinylidene fluoride (PVDF) are weighed and ground according to the mass ratio of 7:2:1, and then dispersed into 240 μL 1-methyl-2-pyrrolidinone (NMP) and stirred with a paint blender to form a uniform ink. Next, an appropriate amount of ink was coated on the treated NF (1.0 x 1.0 cm^2) with a loading of ~2.0 mg cm^{-2}, and then dried for 12 h under vacuum conditions at 80 °C.

The electrocatalytic measurements were conducted by using CHI760E (CH Instruments) with 1.0 M KOH as electrolyte in a standard three electrode system, in which as-prepared catalysts were directly used as working electrode, carbon rod and Hg/HgO electrodes were used as the counter and the reference electrodes, respectively. The reference was calibrated against and converted to the reversible hydrogen electrode (RHE) according to the following Nernst equation: $E_{RHE} = E_{Hg/HgO} + 0.059$ pH $+ 0.098$, $E_{corrected} = E_{RHE} - iR$. Linear sweep voltammograms (LSVs) were

measured from 1.003 to 1.803 V vs. RHE at a scan rate of 2 mV s^{-1} and corrected by iR compensation. The overpotential (η) was obtained though the following formula: $\eta = E_{RHE} - 1.23$ V. Tafel slope was obtained by fitting linear portions of the Tafel plots derived from LSV. Electrochemical impedance spectroscopy (EIS) was estimated in the frequency range from 100 kHz to 0.1 Hz at 1.55 V vs. RHE. Cyclic voltammetry (CV) was used to measure the double-layer capacitance (C_{dl}) at different scan rates of 2, 4, 6, 8 and 10 mV s^{-1} in the non-faradaic region. The electrochemical active surface area (ECSA) normalized current densities was investigated to evaluate the inherent activity of catalysts. The ECSA could be calculated according to the following equation: ECSA = C_{dl} / C_s × S, where the specific capacitance (C_s) is 0.04 mF cm^{-2} and the surface area (S) of NF coated with catalysts is 1 cm^2 in this equation. The long-term stability of catalysts was assessed by LSV, and i-t curve at 10 mA cm^{-2} for 26 h in 1.0 M KOH.

Calculation of the Theoretical OER Activity

Density functional theory calculations were performed on Vienna Ab-initio Simulation Package.[1,2] The exchange-correlation energy and projector augmented wave method was used to represent the core-valence interaction with generalized gradient approximation (GGA) and Perdew-Burke-Ernzerhof (PBE) function.[3,4] DFT + U correction was used to improve the description of d-electrons with U of 4.3 and 3.8 eV for Fe and Ni, respectively. The energy cutoff was set to 400 eV during the calculation. The energy and force criterion were set to 10^{-5} eV and 0.04 eV Å-1, respectively, with K-point mesh of 3 × 3 × 1. Calculations were conducted on a slab model of FeNi-LDH (100) and v-FeNi-LDH (100), with vacuum layers of 12 Å thicknesses.

During the alkaline OER process, there are four elementary steps:

$$OH^- + * \rightarrow *OH + e^- \qquad (1)$$

$$*OH + OH^- \rightarrow *O + H_2O + e^- \qquad (2)$$

$$*O + OH^- \rightarrow *OOH + e^- \qquad (3)$$

$$*OOH + OH^- \rightarrow * + O_2 + e^- \qquad (4)$$
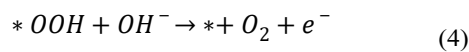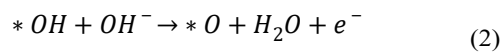
Where * represents the active sites. The free energy of the adsorbed species can be calculated as follows:

$$\Delta G = \Delta E + \Delta ZPE - T\Delta S$$

ZPE and TS were obtained through VASPKIT.[5]

The overpotential η can be obtained from the Gibbs free energy differences of each step,[6] i.e.

$$\eta^{OER} = \frac{\Delta G_{max}}{e} - 1.23V$$
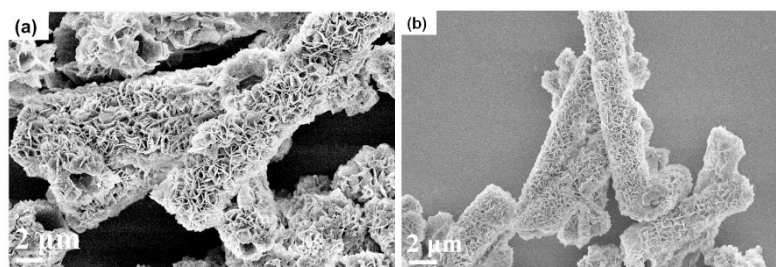
Fig. S1. SEM image of a) Ni precursor microtubes, b) NiFe LDH.
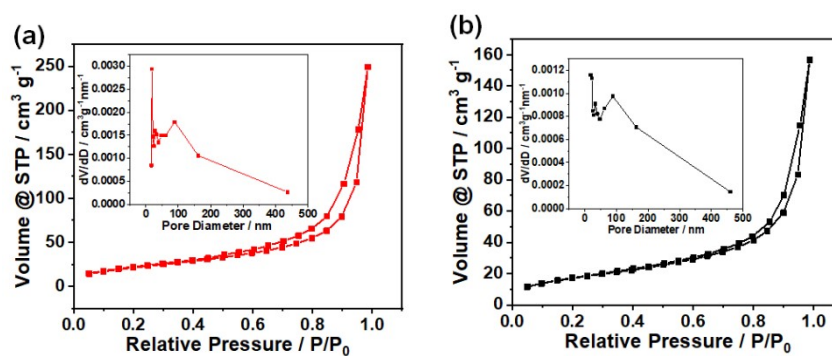
Fig. S2. N$_2$ adsorption-desorption isotherms and corresponding pore size distribution curves of a) v-NiFe LDH, b) NiFe LDH.
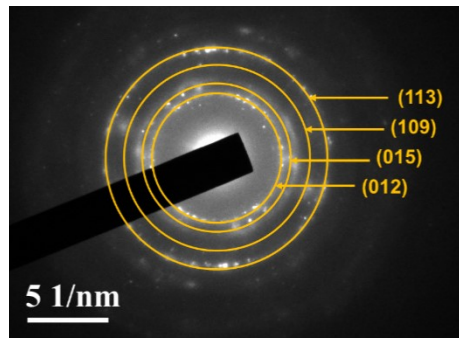
Fig.S3. SAED of v-NiFe LDH.
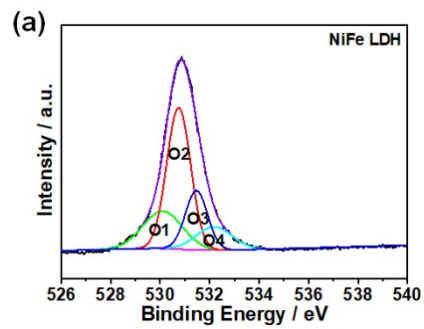
Fig. S4. High-resolution XPS spectra O1s spectra in NiFe LDH.
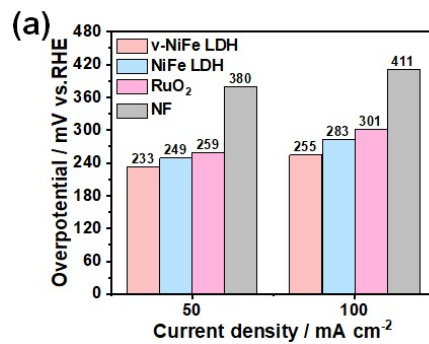
Fig. S5. A bar graph of the corresponding overpotential (η) at 50 and 100 mA cm^{-2} of the v-NiFe LDH, NiFe LDH, RuO$_2$ and NF.
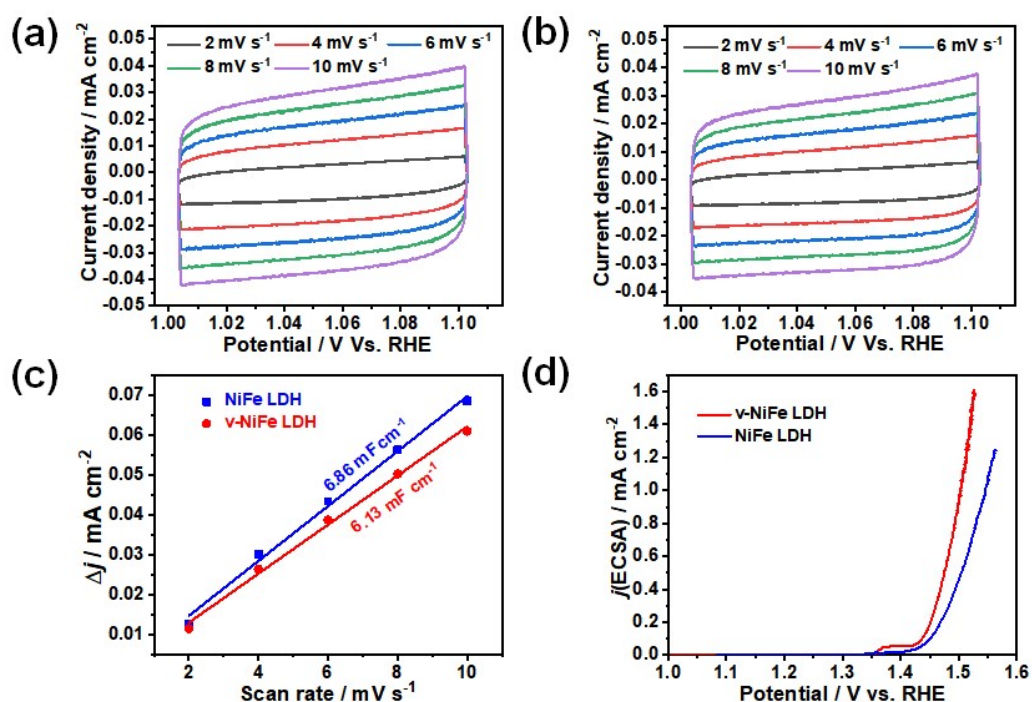
Fig. S6. CV at different scan rates (from 2 mV s-1 to 10 mV s-1). (a) v-NiFe LDH, (b) NiFe LDH. (C) corresponding anodic and cathodic capacitive current density difference ($\Delta j = j_a\text{-}j_c$) at 1.0531 V vs. RHE as a function of scan rate of v-NiFe LDH and NiFe LDH. (d) LSV curves normalized by ECSA.
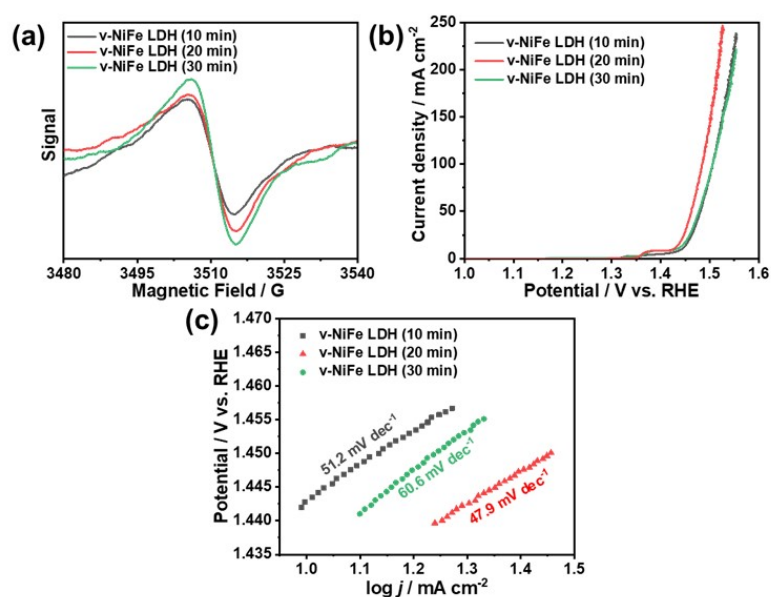
Fig. S7. (a) EPR spectra for v-NiFe LDH under the same NaBH4 solution concentration (1 M) and different immersion time (10 min, 20 min, 30 min). (b) LSV curves. (c) Tafel slope.
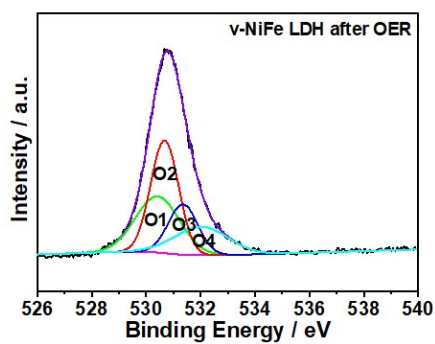
Fig. S8. High-resolution XPS spectra of v-NiFe LDH after 26 h stability test: O1s.
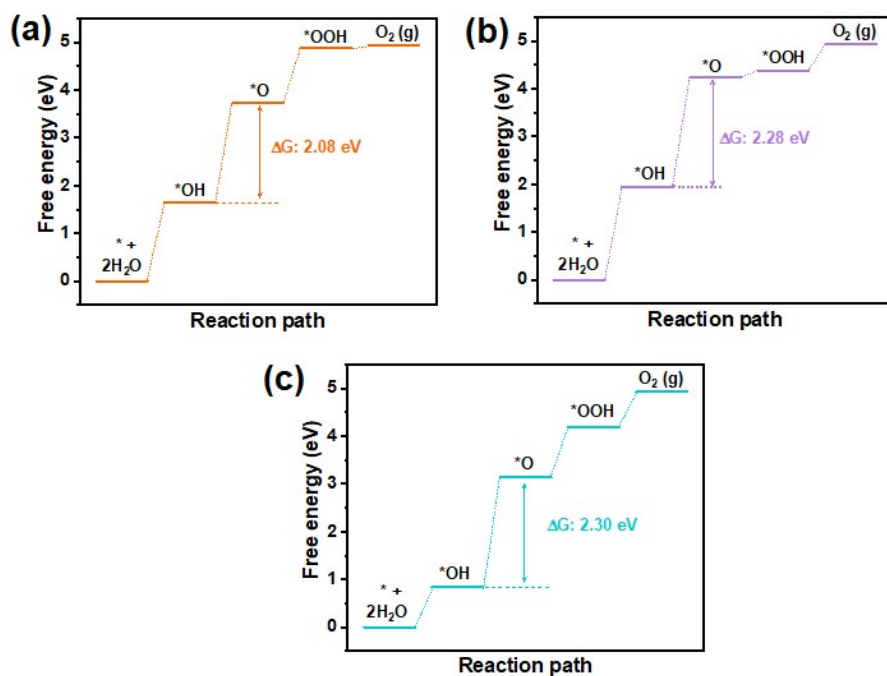
Fig. S9. Theoretical OER Gibbs free energy diagrams (a) Fe site as adsorption site, (b) Ni site as adsorption site and (c) oxygen vacancy as adsorption site of the v-NiFe LDH.
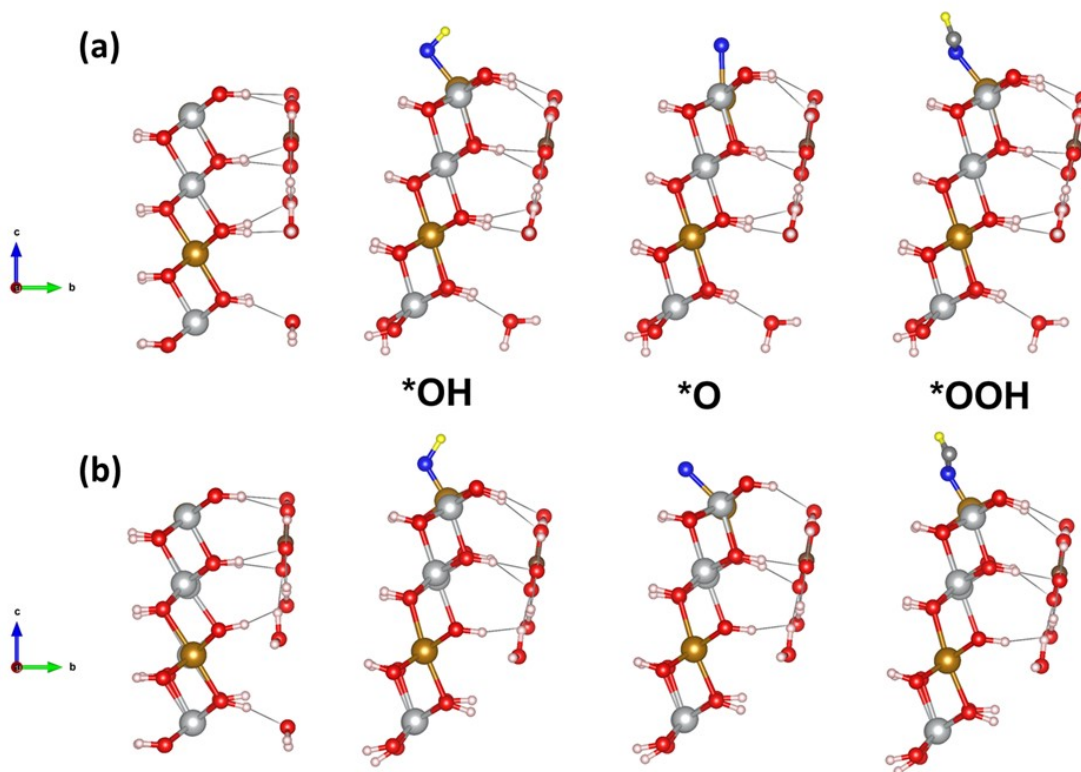
Fig. S10 The optimized geometries of the intermediate products for (a) pristine NiFe LDH (100) and B) v-NiFe LDH (100).

Table S1. the Gibbs free energies (ΔG) of Fe sites on the (100) facets as adsorption site in the NiFe LDH and v-NiFe LDH.

	ΔG_{*OH}/eV	ΔG_{*O}/eV	ΔG_{*OOH}/eV	ΔG_1/eV	ΔG_2/eV	ΔG_3/eV	ΔG_4/eV
NiFe LDH	1.642	3.724	4.872	1.642	2.082	1.148	0.005
v-NiFe LDH	1.703	4.253	4.887	1.703	2.55	0.634	0.035

Table S2. Comparison of the OER activities of the v-Ni-Fe LDH prepared in this work with some recently-reported Ni-Fe based catalysts in alkaline medium.

Catalyst	Electrolyte solution	Tafel slope (mV dec^{-1})	Overpotential at 10 mA cm^{-2} (mV)	Substrate	Ref.
v-NiFe LDHs	1M KOH	47.9	195	NF	our work
NiCo2S4@NiFe LDH	0.1M KOH	86.4	287		7
NiFe LDHs-VFe	1M KOH	70	245	GCE	8
NiFe LDHs-VNi	1M KOH	62.9	229	GCE	8
V-Ni$_3$S$_2$@NiFe LDH	1M KOH	32.5	209		9
v-NiFe LDH	1M KOH	34.8	210	NF	10
Ni$_{0.83}$Fe$_{0.17}$(OH)$_2$	1M KOH	61	245	GCE	11
NiFe-LDH@NiCoP/NF	1M KOH	48.6	220	NF	12
oxygen-enriched NiFe-LDH nanosheets	1M KOH	74.1	310	GC	13
P-Ni$_{0.5}$Fe@C	1M KOH	65	256	GCE	14
FeNi-HDNAs	1M KOH	91	206	RuO$_2$/NF	15
Ni@NiFe LDH	1M KOH	66.3	218	CP	16
NF@Ni/C	1M KOH	54	265	NF	17

Ni5P4/NiP2/NiFe LDH	1M KOH	46.6	197	NF	18
FeNiW-LDH	1M KOH	55.7	202	FeF	19

1   G. Kresse and J. Hafner, *Physical Review B*, 1994, **49**, 14251-14269.

2   G. Kresse and J. Furthmüller, *Physical review B*, 1996, **54**, 11169-11186.

3   J. P. Perdew, K. Burke and M. Ernzerhof, *Phys. Rev. Lett.*, 1996, **77**, 3865-3868.

4   G. Kresse and D. Joubert, *Physical review B*, 1999, **59**, 1758-1775.

5   V. Wang, N. Xu, J.-C. Liu, G. Tang and W.-T. Geng, *Comput. Phys. Commun.*, 2021, **267**, 108033.

6   H. Fei, J. Dong, Y. Feng, C. S. Allen, C. Wan, B. Volosskiy, M. Li, Z. Zhao, Y. Wang and H. J. N. C. Sun, *Nat. Catal.*, 2018, **1**, 63-72.

7   X. Feng, Q. Jiao, W. Chen, Y. Dang, Z. Dai, S. L. Suib, J. Zhang, Y. Zhao, H. Li and C. Feng, *Appl. Catal. B,* 2021, **286**, 119869.

8   Y. Wang, M. Qiao, Y. Li and S. Wang, *Small*, 2018, **14**, 1800136.

9   J. Zhou, L. Yu, Q. Zhu, C. Huang and Y. Yu, *J. Mater. Chem. A*, 2019, **7**, 18118-18125.

10   Y. Wang, S. Tao, H. Lin, G. Wang, K. Zhao, R. Cai, K. Tao, C. Zhang, M. Sun and J. Hu, *Nano Energy*, 2021, **81**, 105606.

11   Q. Zhou, Y. Chen, G. Zhao, Y. Lin, Z. Yu, X. Xu, X. Wang, H. K. Liu, W. Sun and S. X. Dou, *Acs Catalysis*, 2018, **8**, 5382-5390.

12   Z. Sun, Y. Wang, L. Lin, M. Yuan, H. Jiang, R. Long, S. Ge, C. Nan, H. Li and G. Sun, *ChemComm*, 2019, **55**, 1334-1337.

13   H. Chen, Q. Zhao, L. Gao, J. Ran and Y. Hou, *ACS Sustain. Chem. Eng.*, 2019, **7**, 4247-4254.

14   A. Fan, C. Qin, X. Zhang, X. Dai, Z. Dong, C. Luan, L. Yu, J. Ge and F. Gao, *ACS Sustain. Chem. Eng.*, 2018, **7**, 2285-2295.

15   N. Yu, W. Cao, M. Huttula, Y. Kayser, P. Hoenicke, B. Beckhoff, F. Lai, R. Dong, H. Sun and B. Geng, *Appl. Catal. B*, 2020, **261**, 118193.

16   Z. Cai, X. Bu, P. Wang, W. Su, R. Wei, J. C. Ho, J. Yang and X. Wang, *J. Mater. Chem. A*, 2019, **7**, 21722-21729.

17   H. Sun, Y. Lian, C. Yang, L. Xiong, P. Qi, Q. Mu, X. Zhao, J. Guo, Z. Deng and Y. Peng, *Energy & Environmental Science*, 2018, **11**, 2363-2371.

18   L. Yu, H. Zhou, J. Sun, I. K. Mishra, D. Luo, F. Yu, Y. Yu, S. Chen and Z. Ren, *J. Mater. Chem. A*, 2018, **6**, 13619-13623.

19   J. He, X. Zhou, P. Xu and J. Sun, *Nano Energy*, 2021, **80**, 105540.